Journal of King Saud University – Science 33 (2021) 101298

Contents lists available at ScienceDirect

Journal of King Saud University – Science

journal homepage: www.sciencedirect.com

Synthesis, physicochemical, thermal, XDR/HSA-interactions of *Trans*-(1*E*,2*E*)-Benzil-*O*,*O*-dimethylsulfonyl dioxime: Cis-trans isomerization, DFT and TD-DFT investigation

Nabil Al-Zaqri [a,*], Ali Alsalme [a], Fahad Alharthi [a], Afnan Al-Taleb [a], Ahmed M. Boshaala [b], Ahmed Chetouni [c], Abdelkader Zarrouk [d], Ismail Warad [e,*]

[a] Department of Chemistry, College of Science, King Saud University, P.O. Box 2455, Riyadh 11451, Saudi Arabia
[b] Department of Chemistry, Faculty of Science, Benghazi University, P O Box 1308, Benghazi, Libya
[c] Laboratoire de Chimie Analytique Appliquée, Matériaux et Environnement (LC2AME), Faculté des Sciences, Université Mohamed I, 60 000 Oujda, Morocco
[d] Laboratory of Materials, Nanotechnology and Environment, Faculty of Sciences, Mohammed V University, Av. Ibn Battouta, Box 1014 Agdal-Rabat, Morocco
[e] Department of Chemistry, Science College, An-Najah National University, P.O. Box 7, Nablus, Palestine

ARTICLE INFO

Article history:
Received 20 October 2020
Revised 20 November 2020
Accepted 14 December 2020
Available online 24 December 2020

Keywords:
Dioxime
XRD
HSA
MEP
NMR

ABSTRACT

In this study, a novel *trans*-(1*E*,2*E*)-benzil-*O*,*O*-dimethylsulfonyl dioxime (BDMDO) monomer was prepared *via* a one-step dehydrochlorination reaction. BDMDO was characterized by ^{1}H and ^{13}C NMR, UV–Vis, and FT-IR spectroscopies, CHN elemental analysis, mass spectrometry, energy-dispersive X-ray spectroscopy, and TGA. According to the X-ray diffraction data, the BDMDO crystal structure was solved as a *trans*-isomer dioxime. The lattice structure was stabilized by two types of H-bonds and a sufficient number of interesting non-covalent supramolecular interactions such as the C—H···H—C bonds. Molecular electrostatic potential measurements and Hirschfeld surface analysis were performed to understand these interaction modes. The *cis–trans* isomerization in BDMDO as well as the structural, vibrational, NMR, highest occupied molecular orbital/lowest unoccupied molecular orbital bandgap, density of states, and electronic properties were computed by the density functional theory and subsequently compared with available experimental ^{1}H and ^{13}C NMR, UV–Vis, and FT-IR spectral data. The thermogravimetric/derivative thermogravimetric behavior of BDMDO was determined experimentally under an open-room atmosphere.

1. Introduction

Oximes (>C=N-O–H) and their derivatives such as > C=N-O-SO_2-R are useful building blocks in the preparation of organics with SNO polar atoms (Türkkan et al., 2012). Generally, oximes are prepared by the reaction of ketones or aldehydes with hydroxylamine. They are considered as key synthetic precursors because they can be easily converted to carbonyl, amino, nitro, and cyano groups (Özyürek et al., 2014). This makes oximes essential in laboratories, industries, and in our daily life. For example, in Japan, perillaldehyde-oxime or perilla sugar is used as a synthetic sweetener as it is two thousand times sweeter than sucrose (Adebayo et al., 2017). Oximes are also used in medicine to treat organophosphate poisoning as antibiotics such as mesylate, gemi-floxacin obidoxime chloride, and pralidoxime chloride (Türkkan et al., 2012) and as pesticides and fungicides such as diazinon and malathion (Adebayo et al., 2017). In addition to their antifungal, antioxidant, antiviral, and antibacterial properties, oximes reportedly exhibit tumor growth inhibition activities (Adebayo et al., 2017; Türkkan et al., 2012; Lorke et al., 2008; Pohanish, 2017; Aakeröy et al., 2013; Talley et al., 2000). Furthermore, owing to their antioxidant activities, oximes have numerous industrial applications, e.g., in

Abbreviations: DFT, Density functional theory; DOS, Density of states; EDX, Energy-dispersive X-ray; GIAO, Gauge-including atomic orbital; HSA, Hirschfeld surface analysis; MEP, Molecular electrostatic potential; MS, Mass spectrometry; TS, Transition state; XRD, X-ray diffraction.

* Corresponding authors.
E-mail addresses: nalzaqri@ksu.edu.sa (N. Al-Zaqri), warad@najah.edu (I. Warad).

Peer review under responsibility of King Saud University.

Production and hosting by Elsevier

https://doi.org/10.1016/j.jksus.2020.101298
1018-3647/

Table 1
Experimental details.

Chemical formula	$C_{16}H_{16}N_2O_6S_2$
CCDC	794,517
M_r	396.43
Crystal system, space group	Triclinic, *P*
Temp. (K)	293
a, *b*, *c* (Å)	5.392 (2), 9.300 (4), 9.420 (4)
α, β, γ (°)	93.933 (9), 90.198 (11), 106.375 (9)
Z	4
V (Å^3)	452.0 (3)
μ (mm^{-1})	0.33
Radiation type	Mo *K*α
Diffractometer	Rigaku RAXIS-RAPID
Crystal size (mm)	0.50 × 0.20 × 0.20
No. of measured, independent, and observed [$I > 2\sigma(I)$] reflections	2059, 2059, 1741
R_{int}	0.052
θ_{max} (°)	58.8
$(\sin\theta/\lambda)_{max}$ (Å^{-1})	0.649
$R[F^2 > 2\sigma(F^2)]$, $wR(F^2)$, *S*	0.047, 0.157, 1.05
No. of reflections, parameters	2059, 119
$\Delta\rho_{max}$, $\Delta\rho_{min}$ (e Å^{-3})	0.33, −0.43

plastics, textiles, detergents, radical scavengers, and paint materials(Talley et al., 2000; Türkkan et al., 2012; Adebayo et al., 2017; Lorke et al., 2008; Pohanish, 2017). The chelating properties of oximes expand their applications and have attracted attention relating to their use as polar polydentate ligands. In this role, oximes have been used to evaluate metal ions in environmental samples, e.g., uranium in seawater, nickel and cobalt in tap water and those

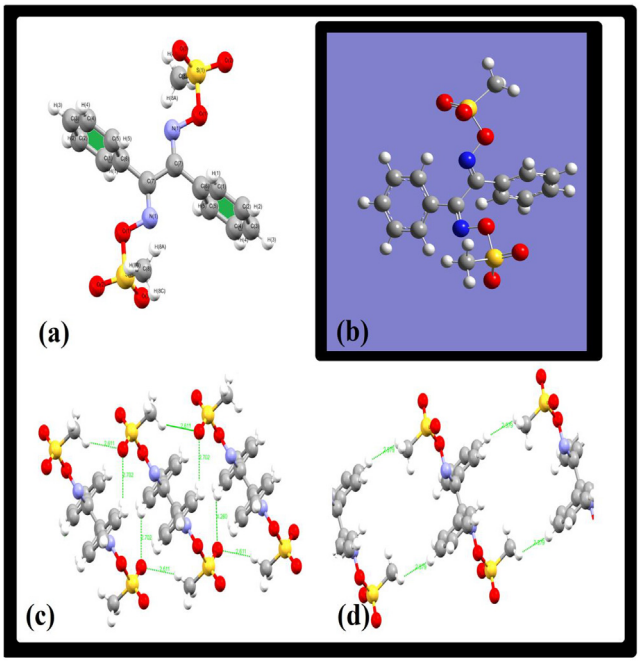

Fig. 2. (a) ORTEP and (b) optimized B3LYP/6-311G(d) structures of BDMDO, and (c) H-bonds and (d) C—H···H—C bond interactions.

present in plant foodstuffs and meat (Görgülü and Dede, 2019; Zengin et al., 2019; Motaleb and Selim, 2019; Warad et al., 2018a). Moreover, metal complexes using oximes as ligands have been used as catalysts because of their mode of coordination and

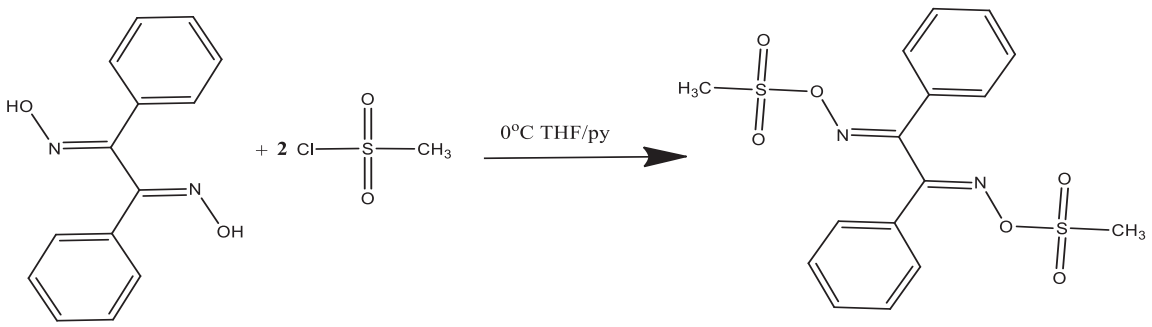

Scheme 1. Synthesis of BDMDO.

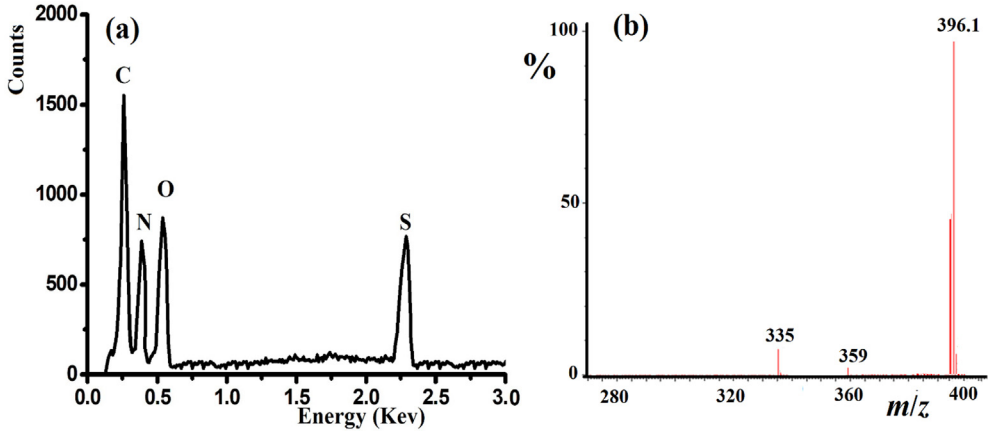

Fig. 1. (a) EDX and (b) MS of DMDO.

Table 2
Selected experimental XRD and DFT-B3LYP calculated angles and bond lengths.

Bond no.	Bond (Å)		Exp. XRD	DFT/B3LYP	Angles no.	Angles (°)			Exp. XRD	DFT/B3LYP
1	S(1)	O(1)	1.618(2)	1.6907	1	O(1)	S(1)	O(2)	101.8(1)	108.44
2	S(1)	O(2)	1.412(2)	1.4589	2	O(1)	S(1)	O(3)	110.0(1)	109.68
3	S(1)	O(3)	1.413(2)	1.4564	3	O(1)	S(1)	C(8)	102.3(1)	94.24
4	S(1)	C(8)	1.743(2)	1.7969	4	O(2)	S(1)	O(3)	120.1(1)	121.15
5	O(1)	N(1)	1.438(3)	1.4266	5	O(2)	S(1)	C(8)	111.0(1)	110.04
6	N(1)	C(7)	1.281(3)	1.2857	6	O(3)	S(1)	C(8)	109.9(1)	109.94
7	C(1)	C(2)	1.383(4)	1.395	7	S(1)	O(1)	N(1)	110.3(1)	110.25
8	C(1)	C(6)	1.372(3)	1.3782	8	O(1)	N(1)	C(7)	109.3(2)	110.96
9	C(2)	C(3)	1.352(4)	1.3556	9	C(2)	C(1)	C(6)	119.9(2)	119.28
10	C(3)	C(4)	1.353(4)	1.3544	10	C(6)	C(7)	C(7)	120.8(2)	121.22

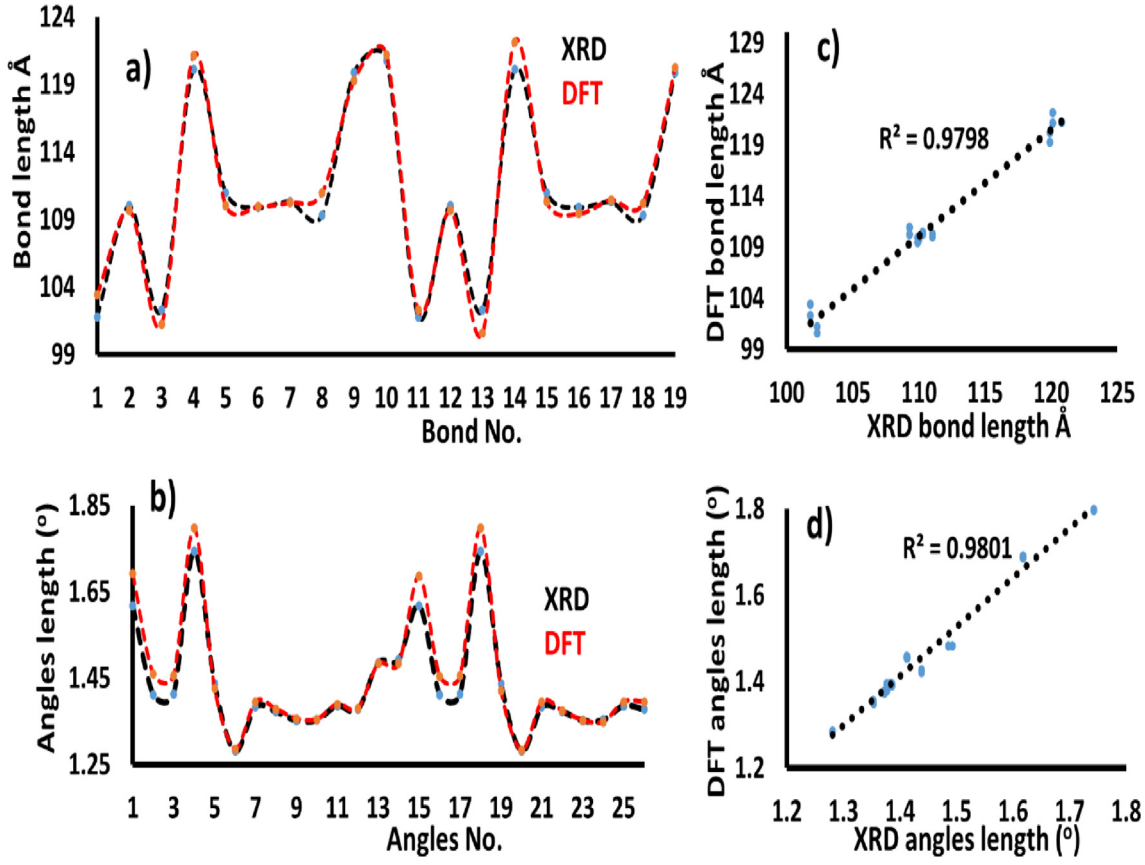

Fig. 3. (a) XRD/DFT bond length relation and its graphical correlation; (b), (c) DFT/XRD angle relation and its graphical correlation (d).

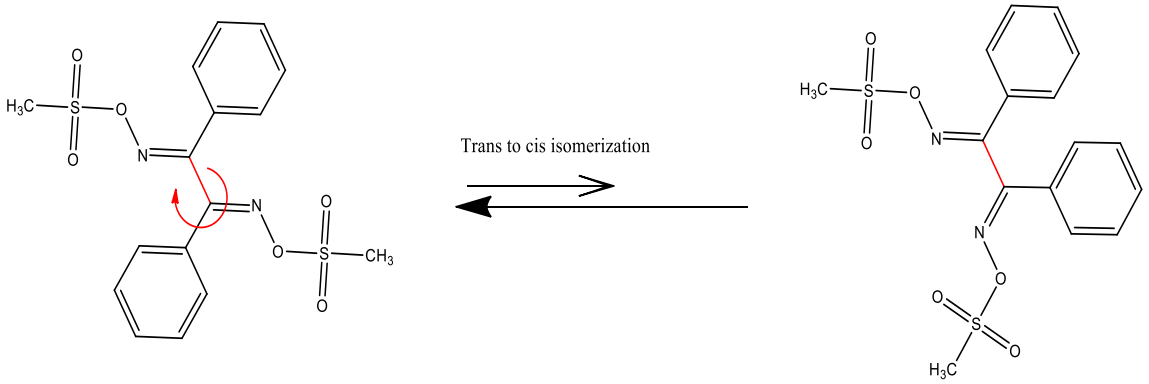

Scheme 2. *Trans–cis* isomerization studied by DFT.

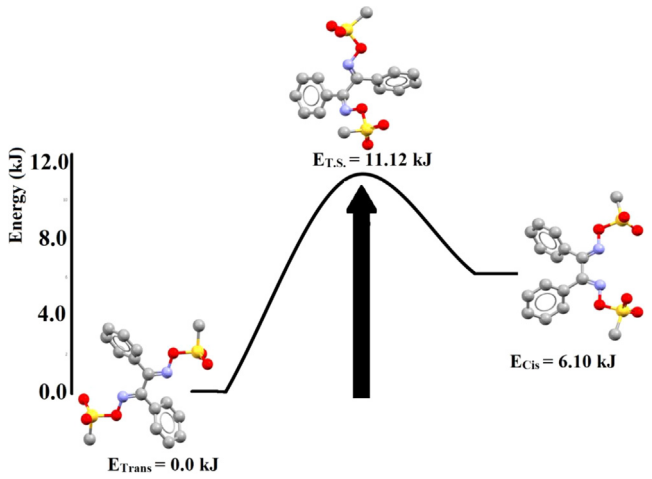

Fig. 4. Energy and structure profiles of *trans*–[TS_{QTS2}]–*cis* isomerization.

structural stability (Gup et al., 2017; Stoumpos et al., 2010; Westcott et al., 2016; Bulatov et al., 2014). Information pertaining to the energetic, structural, molecular, vibrational, magnetic, and electronic behavior of these compounds has been obtained by the density functional theory (DFT), which has facilitated investigation into the design, synthesis, and characterization of novel materials based on oximes (Aouad et al., 2018).

To the best of our knowledge, neither the experimental spectra of *trans*-(1*E*,2*E*)-benzil-*O*,*O*-dimethylsulfonyl dioxime (BDMDO) nor DFT-quantum chemical calculations have been reported to date. In this study, we have reported the synthesis and characterization of the *trans*-dioxime, DMDO. The DFT/experimental structural and spectral parameters were matched in this study. Hirschfeld surface analysis (HSA) and molecular electrostatic potential (MEP) computational analysis were employed to understand the X-ray diffraction (XRD) packing connections. The *cis*–*trans* isomerization process was computed successfully by DFT. The thermal behavior of the desired dioxime was determined experimentally using thermogravimetry/derivative thermogravimetry (TG/DTG).

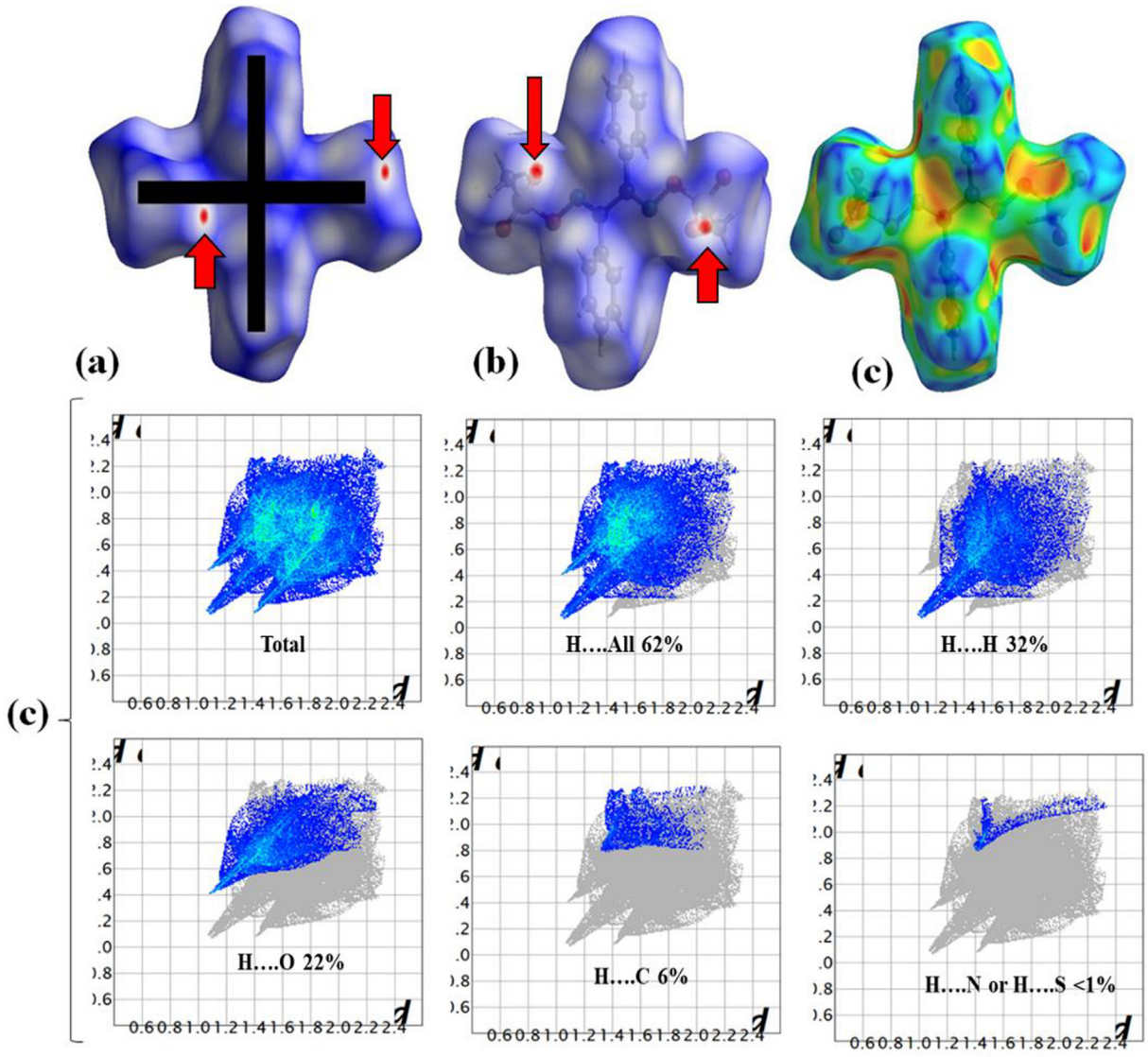

Fig. 5. (a) dnorm, (b) shape index, (c) curvedness structures, and (d) inside/outside 2D-FP plot of BDMDO.

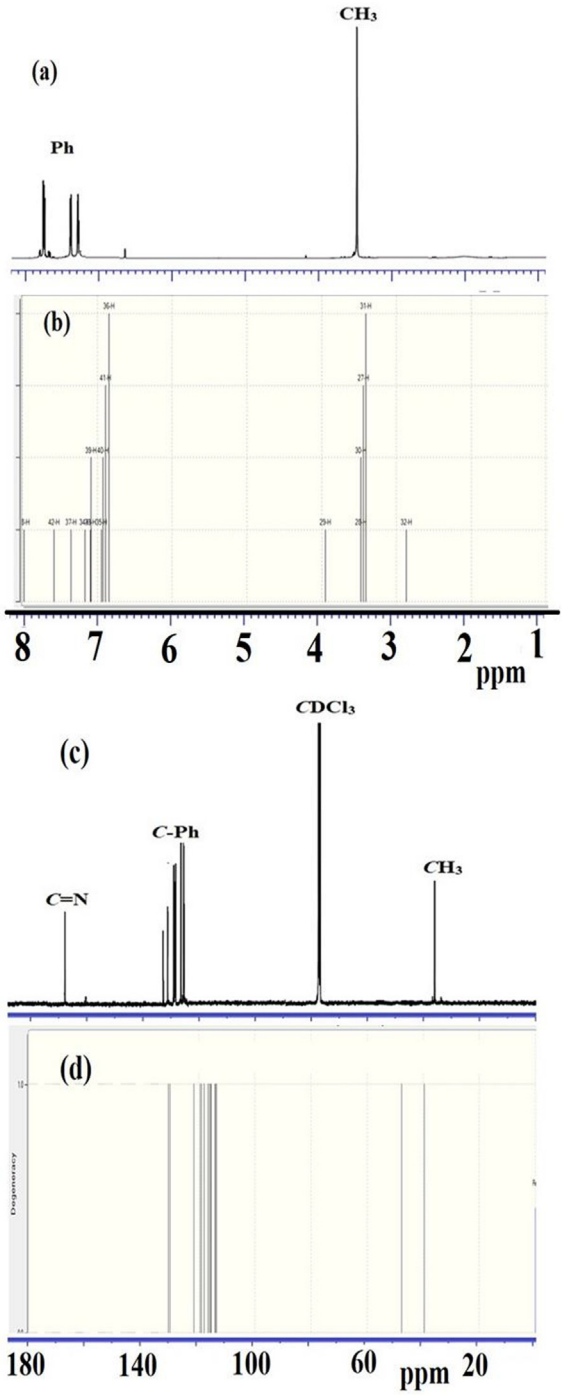

Fig. 6. ^{1}H NMR: (a) experimental and (b) GIAO, and ^{13}C NMR: (c) experimental and (d) GIOA spectra of BDMDO.

2. Experimental section

2.1. Instruments, software, and calculations

The chemicals used in this study were purchased from Sigma-Aldrich Chemicals and used as received. The XRD structural analysis was performed on a Rigaku RAXIS-RAPID 1000 diffractometer fitted with a charge-coupled device. The UV–Vis analysis was conducted on a Thermo Scientific Genesys 10 s spectrophotometer. Mass spectrometry (MS) measurements were conducted on a Varian MAT 711 spectrometer. The CHN elemental analysis was conducted using Perkin-Elmer Series I1 CHNSlO Analyzer 2400 and IR analysis was performed using a Nicolet Nexus spectrometer. The ^{1}H and ^{13}C NMR spectra were recorded on a JEOL ECS 400 or LAMBDA 400 spectrometer. DFT calculations at the B3LYP level of theory with a 6–311 G(p) basis set were performed using the Gaussian09 software (Wolff et al., 2012). The XRD structure was solved and refined using the SHELXT program)Sheldrick, 1997) and HSA was carried out using the CRYSTAL EXPLORER 3.1 software (Frisch et al., 2009).

2.2. Synthesis

A portion of methanesulfonyl chloride (0.8 g, 7.2 mmol) was dissolved in a mixture of 8 mL of pyridine and 40 mL of tetrahydrofuran (THF). The solution was cooled to −5 °C, and treated dropwise with 0.84 g (3.5 mmol) of diphenylglyoxime in THF for 1 h. The mixture was continuously stirred for 6 h at room temperature, and subsequently treated with 40 mL of dichloromethane and 200 mL of water in a 500 mL separating funnel. The dichloromethane layer was separated, followed by evaporation to obtain the desired product as white crystals in 80% yield (Warad et al., 2010). ^{1}H NMR ($CDCl_3$, ppm): δ 3.5 (s, 6H), 7.2–8.0 (3 m, 10*H*-ph), ^{13}C NMR δ 28.0 ($2CH_3$), 120.0–130.0 (12C-ph), 134.5 (2C=N) (See Table 1).

3. Results and discussion

3.1. Synthesis, CHN elemental analysis, and energy-dispersive X-ray (EDX) analyses

BDMDO was synthesized by the dehydrogenation of 1 equiv. of (1*E*,2*E*)-benzil dioxime and 2 equiv. of methanesulfonyl chloride in dry THF using pyridine as a soft base. The elemental analysis indicated the theoretical values for the formation of a 1:2 mononuclear dioxime, as shown in Scheme 1.

The EDX analysis results reflected the stereochemistry of the components that combined to form DMDO. The EDX analysis results of the BDMDO structure indicated the presence of four types of atoms, including S, O, N, and C atoms, in its backbone, as shown in Fig. 1a.

The MS results of BDMDO (m/z = 396.1 (observed), 396.52 (theoretical), Fig. 1b), exhibited sufficient correlation with $C_{16}H_{16}N_2O_6S_2$: Anal. Calcd C, 48.47; H, 4.07; N, 7.07, found: C, 48.36; H, 4.08; N, 7.01%.

3.2. X-ray single crystal diffraction and DFT calculations

The ORTEP and DFT-optimized structures of BDMDO are illustrated in Fig. 2a and b, respectively. The bond length and angle values obtained by DFT and XRD are summarized in Table 2. BDMDO was crystallized in the lattice with triclinic and P space groups without any solvent molecules in the crystal lattice. Only the *anti*-isomer was detected by XRD, where the N–SO_2CH_3 functional groups were pointed far away from each other because of steric hindrance. No sterically disfavored *syn* isomer was detected by XRD, which is consistent with the previous report of the *cis* oxime being the less stable isomer [24]. The C═N—O—S torsion angle of 177.8° indicated a preference for close planarity; the N═C···C═N dihedral angle was found to be 180°, which is assumed to be a stable *trans*-conformation isomer of BDMDO. The S-O, O—N, and C═N bond lengths of 1.619, 1.438, and 1.281 Å, respectively, and the O—N═C, S—O—N, and S—O—C angles of 109.32°, 110.26°, and 102.25°, respectively, were consistent with literature data (Plater et al., 2019). In the XRD packing system, the BDMDO molecules were linked by 2H-bond types, such as C_{Ph}-H···O=SO_2- and C_{Me}-

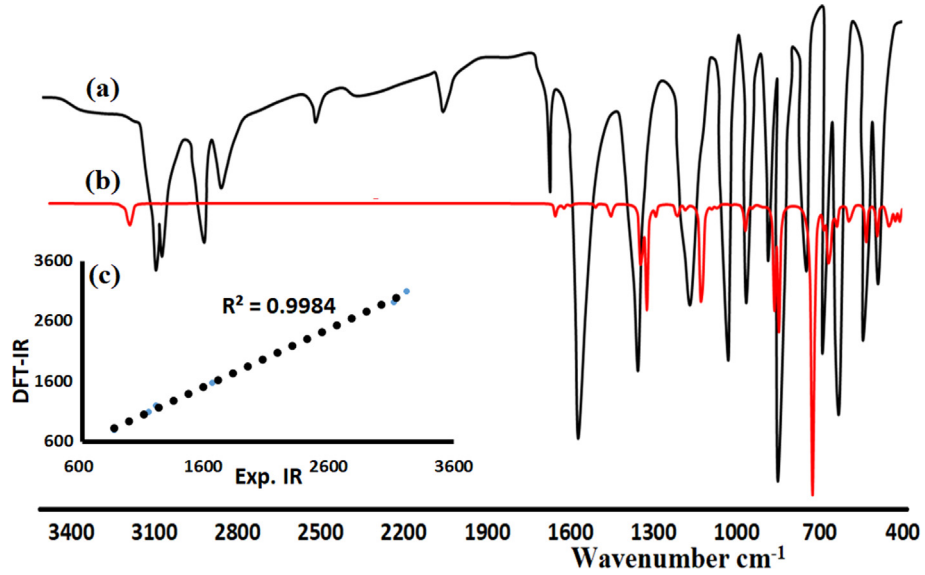

Fig. 7. Infrared spectra of BDMDO: (a) Experimental, (b) B3LYP/IR, and (c) Exp./DFT relation.

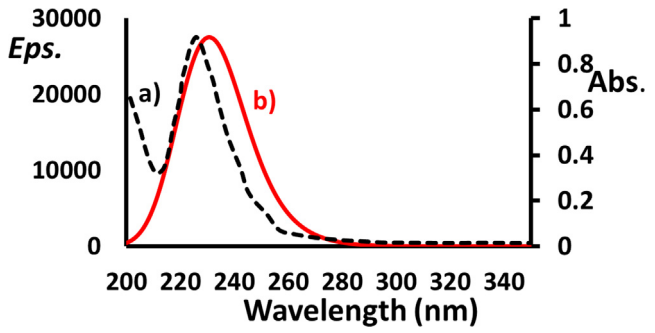

Fig. 8. UV–Visible and TD-DFT spectra of BDMDO in MeOH.

H···O=SO_2- with 2.611 and 2.702 Å bond lengths, respectively, as shown in Fig. 2c, and interesting supramolecular non-covalent interactions such as C—H···H—C bonds with a bond length of 2.378 Å, as shown in Fig. 2d.

There was an excellent agreement between the DFT/XRD bond lengths and angles, as shown in Fig. 3a and c, respectively. The graphical correlation (R^2) of the bonds is 0.9798 (Fig. 3b), while that of the angles is 0.9801 (Fig. 2d). Thus, a significant correlation was established between the XRD/DFT structural parameters.

3.3. Trans–cis isomerization in DMDO

Based on the analysis of the XRD patterns recorded in this study, the *trans*-isomer was preferentially isolated over the *cis*-isomer in accordance with steric effect rules. As other researchers have been able to detect *cis* isomers of oximes by XRD, we believe that it is possible for the dioxime to be isomerized from *trans* to *cis* under mild conditions.

Therefore, in the gaseous state and by ignoring any molecular interaction, the *trans–cis* isomerization in BDMDO was simulated using DFT/B3LYP/6-311G(d) via a 180° flip rotation around the highlighted Csp^2–Csp^2 bond, as shown in Scheme 2. The transition state (TS) structure of BDMDO was investigated using the QTS2 model. The stereo-chemical variation between the *trans* and *cis* isomers was simulated by performing a 180° flip rotation around the highlighted N═C*···C*═N sp^2–sp^2 bond; a dramatic change occurred in the dihedral angle of *trans* N═C···C═N from 180° to 0° as in the *cis*-isomer; meanwhile, the DFT/QTS2 system TS dihedral angle was found to be ~ 90°. The global-minimum energy of the *trans*-isomer was determined to be – 1976.31730871 a.u. with E_{trans} = 0.0 kJ (zero reference energy) as it was more stable compared to the *cis*-isomer. Meanwhile, the global-minimum energy of the *cis*-isomer was determined to be – 1976.31495695 a.u. with E_{cis} = 6.10 kJ. The energy of the TS was found to be – 1976.3130 7314 a.u. with E_{TS} = 11.12 kJ. The TS structure was recorded in between the *trans–cis* structures with a N═C···C═N dihedral angle of ~ 90°. The isomer energy profile was consistent with the XRD result since it displayed the *trans*-isomer as the more stable isomer (less sterically hindered) as compared to the *cis*-isomer (more steric hindrance). The *trans–cis* isomerization energy in the gaseous state was very low, which is not surprising because a simple 180° single bond Csp^2–Csp^2 flip rotation was performed, as shown in Fig. 4.

3.4. Hirschfield and fingerprint (FP) surface computation

The calculations for elucidating HSA and FP(Titi et al., 2020; Barakat et al., 2018; Warad et al., 2018b; Aouad et al., 2019) of the molecular surface interactions in BDMDO were performed using the original crystallographic information (Fig. 5). The HSA result reflected the formation of a cross-like structure with four red points around the O atoms, which built the O···H bonds. No N···H bonds were detected, which supports the XRD packing result. The percentage ratio of atom···atom FP contacts decrease in the order of H···H (32.0%) > H···O (22%) > H···C (6%) > H···N and H···S (<1%), as shown in Fig. 5d.

3.5. NMR investigation

The σ bonds for the C and H atoms in BDMDO are theoretically supported by the gauge-including atomic orbital (GIAO) approach, and the experiments were performed with $CDCl_3$ as the solvent. The ^{1}H NMR spectrum showed a signal at 3.5 ppm, corresponding to the CH_3 group of methylsulfonyl, and three peaks, which belonged to the aromatic hydrogen between 7.2 and 8.0 ppm, as illustrated in Fig. 6a. The GIAO calculated σ_H reveals an excellent

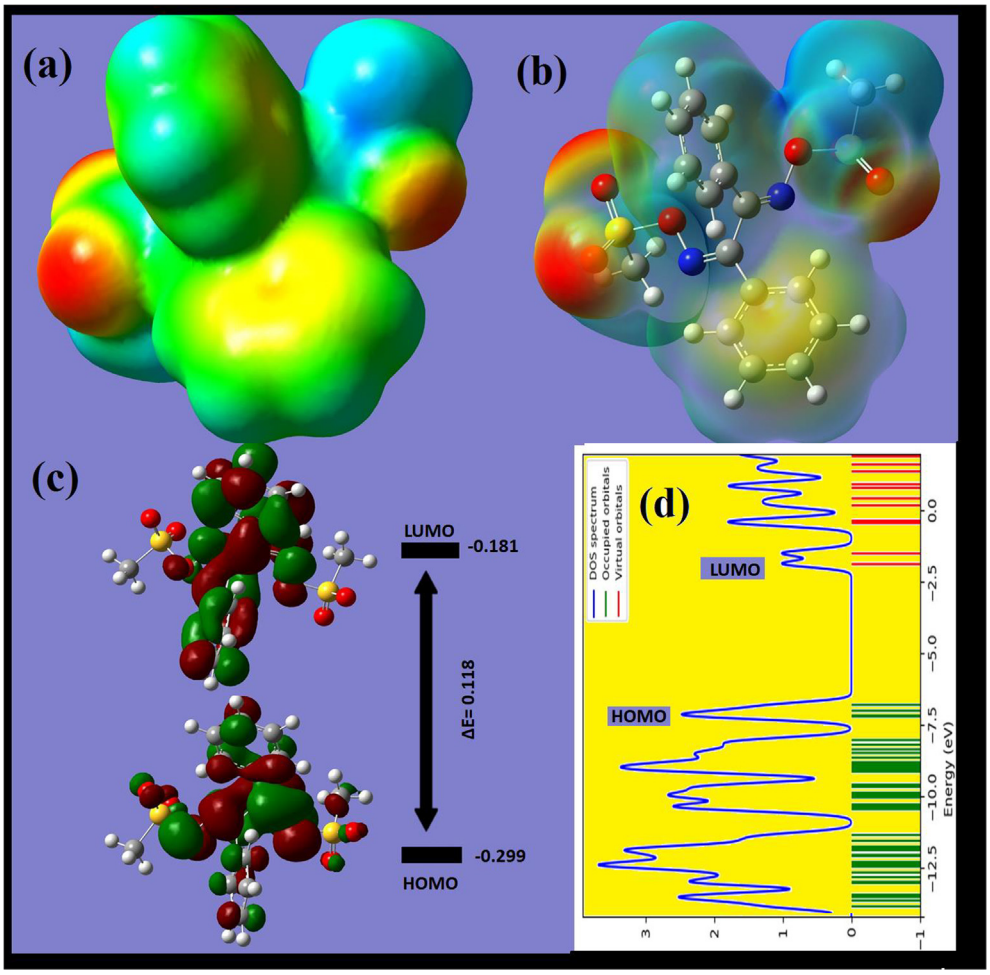

Fig. 9. (a, b) MEP, (c) HOMO/LUMO energy gap, and (d) density of states of BDMDO.

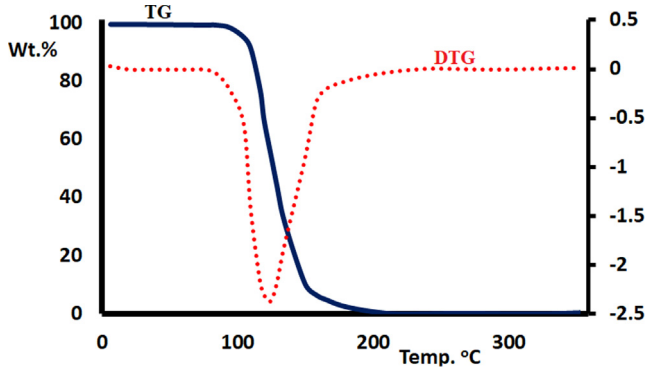

Fig. 10. TG/DTG curves of BDMDO.

correlation with the corresponding experimental result, as shown in Fig. 6b (σ_H of CH_3 is ~ 3.45 and σ_H of H-Ph is ~ 7–8 ppm).

The experimental ^{13}C NMR spectrum showed one signal for three carbons in the aliphatic region corresponding to the CH_3 group at 28 ppm, six signals corresponding to 12C-Ph at 120–130 ppm, and one signal corresponding to two carbons of C=N at 165 ppm, as shown in Fig. 6c. The GIAO calculated carbon chemical shifts revealed a good correlation with the experimental result except for the C=N carbon, which was observed at 134.5 ppm, as shown in Fig. 6d.

3.6. Experimental/DFT–IR investigation

The experimental IR spectrum of BDMDO exhibited many bands corresponding to C_{Ph-H}, C_{Me}-H, C=N, S=O, N—O, S—O, and S—C stretching vibrations. The stretching vibrations of the main functional groups are indicated as follows: the broadest band in the BDMDO spectra was assigned to $\upsilon_{C=N}$ at 1602 cm^{-1}; aromatics exhibited multiple bands in the 3110–3020 cm^{-1} region due to C_{Ph-H}. For the methoxy group, C_{Me}-H appeared in the 2880–2800 cm^{-1} range, and the sulfonyl group S=O bands appeared in the 1380–1260 cm^{-1} range. Other functional groups were assigned to their expected positions, as shown in Fig. 7a. The IR scaled following the DFT/B3LYP/6-311G(p) method was found to be close to the experimental result (Fig. 7b). The DFT frequencies were slightly higher than those obtained from the experimental IR analysis because the B3LYP-IR was computed in the gaseous state, while the experimental IR analysis was performed in the solid-state. In general, an excellent correlation was observed between the experimental and DFT/IR analyses, as evidenced by the correlation coefficient of 0.9984 (see Fig. 7c).

3.7. UV–Visible and TD-DFT/B3LYP comparison

The UV–Visible spectral measurements and time-dependent DFT (TD-DFT) calculations using B3LYP exchange correlation functional with 6-311G(p) basis set were performed on BDMDO in methanol and combined as shown in Fig. 8. The observed and

DFT-predicted wavelengths were in the UV region. In the experimental UV–Vis spectrum, only a $\pi \rightarrow \pi^*$ broad electron band with λ_{max} = 225 nm was recorded and there was no other peak in the visible area. The TD-DFT spectrum was consistent with this observation but with a very small red-shift (λ_{max} = 228 nm with $\Delta\lambda$ = 3 nm) (Fig. 8b). The TD-DFT peak corresponds mainly to the electron transitions from HOMO to LUMO.

3.8. MEP, HOMO/LUMO, and density of states

The MEP is one of the best theoretical methods for predicting the reactive centers in molecules. It was plotted for BDMDO as shown in Fig. 9a. The electron-rich (negative charge) area is indicated with red color around the O atoms, while the positive charge (electron-poor) area is highlighted with blue color around the methyl protons. The red color of the O region is very suitable for electrophilic attack by the blue-colored electrophilic protons to form H···O bonds. The green predominant regions correspond to a potential halfway (red and blue region) in between and do not induce sufficient binding. Such results match well with the XRD and HSA results. The HOMO/LUMO molecular orbital shapes and energy levels were computed using DFTB3LYP/6-311G(d), as illustrated in Fig. 9b. The computed fragment molecular orbital provided sufficient information about the HOMO/LUMO energy gap, $\Delta E_{LUMO-HOMO}$, and the electronic properties of the HOMO and LUMO (Bulatov et al., 2014; Aouad et al., 2018; Wolff et al., 2012; Sheldrick, 1997; Frisch et al., 2009; Warad et al., 2010; Plater et al., 2019). The chemical reactivity of the systems corresponds to the $\Delta E_{LUMO-HOMO}$ value and is associated with the chemical stability of the molecules. Since both HOMO and LUMO have negative energy values, BDMDO should have been stabilized; moreover, the $\Delta E_{LUMO-HOMO}$ was found to be 0.118 a.u. with 3.211 eV, which is a very small energy gap that facelifted the electron in accordance with the π-electrons of the 2C = N conjugation structural system. The small energy gap increased the chemical reactivity, softness, and polarizability of the desired compound [24]. The value of ΔE_{gap} = 3.22 eV obtained by the DOS calculation (Fig. 9d) is consistent with the energy level calculated by the HOMO/LUMO method.

3.9. Thermogravimetric analysis

The thermogravimetric/derivative thermogravimetric (TG/DTG) analysis of BDMDO showed one stage of decomposition pattern from 25 to 350 °C in an open-air O_2 atmosphere at a heating rate of 10 °C/min. Below 105 °C, BDMDO displayed high thermal stability (Fig. 10). The compound was thermally de-structured in broad steps in the range of 110–200 °C with one T_{DTG} = 130 °C. Therefore, BDMDO was completely decomposed, and consequently, zero residue weight was detected at T > 200 °C.

4. Conclusion

In this study, BDMDO was synthesized and fully characterized. The XRD results of BDMDO confirmed the formation of a *trans*-isomer. DFT studies supported the XRD results and the possibility of *trans–cis* isomerization as the energy between the two isomers was low. The QTS2 model reflected the TS with a N═C···C═N dihedral angle of ~90°. The supramolecular assemblies supported the formation of non-covalent C—H···H—C and H-bond interactions in the molecular lattice; such interactions were successfully computed by MEP and HSA. The NMR spectra sufficiently matched their corresponding DFT/6-311G(d) parameters, such as HOMO–LUMO, TD-SCF, B3LYP/IR, and GIAO NMR. The optimized DFT/B3LYP/6-311G(d) structural parameters also correlated well with the experimental XRD data. The TG/DTG behavior reflected the good thermal stability of the dioxime and revealed that it decomposed via a single-step mechanism.

Declaration of Competing Interest

The authors declare that they have no known competing financial interests or personal relationships that could have appeared to influence the work reported in this paper.

Acknowledgements

The authors extend their appreciation to the Deputyship for Research & Innovation, "Ministry of Education" in Saudi Arabia for funding this research work through the project number IFKSURG-1440-141.

References

Aakeröy, C.B., Sinha, A.S., Epa, K.N., Chopade, P.D., Smith, M.M., Desper, J., 2013. Structural chemistry of oximes. Cryst. Growth Des. 13 (6), 2687–2695. https://doi.org/10.1021/cg4005246.

Adebayo, O.A., Abboud, K.A., Christou, G., 2017. New mixed-valence MnII4MnIV clusters from an unusual ligand transformation. Polyhedron 122, 71–78. https://doi.org/10.1016/j.poly.2016.10.018.

Aouad, M.R., Messali, M., Rezki, N., Al-Zaqri, N., Warad, I., 2018. Single proton intramigration in novel 4-phenyl-3-((4-phenyl-1H-1,2,3-triazol-1-yl)methyl)-1H-1,2,4-triazole-5(4H)-thione: XRD-crystal interactions, physicochemical, thermal, Hirshfeld surface, DFT realization of thiol/thione tautomerism. J. Mol. Liq. 264, 621–630. https://doi.org/10.1016/j.molliq.2018.05.085.

Aouad, M.R., Messali, M., Rezki, N., Said, M.A., Lentz, D., Zubaydi, L., Warad, I., 2019. Hydrophobic pocket docking, double-proton prototropic tautomerism in contradiction to single-proton transfer in thione ⇔thiol Schiff base with triazole-thione moiety: Green synthesis, XRD and DFT-analysis. J. Mol. Struct. 1180, 455–461. https://doi.org/10.1016/j.molstruc.2018.12.010.

Barakat, A., Islam, M.S., Al-Majid, A.M., Ghabbour, H.A., Atef, S., Zarrouk, A., Warad, I., 2018. Quantum chemical insight into the molecular structure of L-chemosensor 1,3-dimethyl-5-(thien-2-ylmethylene)-pyrimidine-2,4,6-(1 H ,3 H ,5 H)-trione: Naked-eye colorimetric detection of copper(II) anions. J. Theor. Comput. Chem. 17 (01), 1850005. https://doi.org/10.1142/S0219633618500050.

Bulatov, E.Y., Chulkova, T.G., Boyarskaya, I.A., Kondratiev, V.V., Haukka, M., Kukushkin, V.Y., 2014. Triple associates based on (oxime)Pt(II) species, 18-crown-6, and water: synthesis, structural characterization, and DFT study. J. Mol. Struct. 1068, 176–181. https://doi.org/10.1016/j.molstruc.2014.04.010.

Frisch, M., Trucks, G.W., Schlegel, H.B., Scuseria, G.E., Robb, M.A., Cheeseman, J.R., Scalmani, G., Barone, V., Mennucci, B., Petersson, Ga., 2009. gaussian 09, Revision d. 01, Gaussian. Inc., Wallingford CT 201.

Görgülü, G., Dede, B., 2019. Synthesis, characterization, theoretical calculations and biochemical evaluation of a novel oxime ligand with complexes. J. Mol. Liq. 284, 473–491. https://doi.org/10.1016/j.molliq.2019.03.169.

Gup, R., Erer, O., Dilek, N., 2017. One-pot synthesis of a new 2-substituted 1,2,3-triazole 1-oxide derivative from dipyridyl ketone and isonitrosoacetophenone hydrazone: Nickel(II) complex, DNA binding and cleavage properties. Bioorg. Chem. 71, 325–334. https://doi.org/10.1016/j.bioorg.2017.03.003.

Lorke, D., Kalasz, H., Petroianu, G., Tekes, K., 2008. Entry of oximes into the brain: a review. Curr. Med. Chem. 15, 743–753. https://doi.org/10.2174/092986708783955563.

Motaleb, M.A., Selim, A.A., 2019. Dioximes: synthesis and biomedical applications. Bioorg. Chem. 82, 145–155. https://doi.org/10.1016/j.bioorg.2018.10.011.

Özyürek, M., Akpınar, D., Bener, M., Türkkan, B., Güçlü, K., Apak, R., 2014. Novel oxime based flavanone, naringin-oxime: synthesis, characterization and screening for antioxidant activity. Chem. Biol. Interact. 212, 40–46. https://doi.org/10.1016/j.cbi.2014.01.017.

Plater, M.J., Harrison, W.TA., Killah, R., 2019. Potential photoacid generators based on oxime sulfonates. J. Chem. Res. 43 (1-2), 26–33. https://doi.org/10.1177/1747519819831829.

Pohanish, R.P., 2017. In: Sittig's Handbook of Toxic and Hazardous Chemicals and Carcinogens. Elsevier, pp. 336–580. https://doi.org/10.1016/B978-0-323-38968-6.00002-8.

Sheldrick, G.M., 1997. Program for crystal-structure refinement. SHELX-97.

Stoumpos, C.C., Inglis, R., Roubeau, O., Sartzi, H., Kitos, A.A., Milios, C.J., Aromí, G., Tasiopoulos, A.J., Nastopoulos, V., Brechin, E.K., Perlepes, S.P., 2010. Rare oxidation-state combinations and unusual structural motifs in hexanuclear Mn complexes using 2-pyridyloximate ligands. Inorg. Chem. 49 (10), 4388–4390. https://doi.org/10.1021/ic100089y.

Talley, J.J., Brown, D.L., Carter, J.S., Graneto, M.J., Koboldt, C.M., Masferrer, J.L., Perkins, W.E., Rogers, R.S., Shaffer, A.F., Zhang, Y.Y., Zweifel, B.S., Seibert, K., 2000. 4-[5-Methyl-3-phenylisoxazol-4-yl]-benzenesulfonamide, Valdecoxib: a

potent and selective inhibitor of COX-2 [4]. J. Med. Chem. 43, 775–777. https://doi.org/10.1021/jm990577v.

Titi, A., Shiga, T., Oshio, H., Touzani, R., Hammouti, B., Mouslim, M., Warad, I., 2020. Synthesis of novel Cl2Co4L6 clusterusing 1-hydroxymethyl-3,5-dimethylpyrazole (LH) ligand: Crystal structure, spectral, thermal, Hirschfeld surface analysis and catalytic oxidation evaluation. J. Mol. Struct. 1199, 126995. https://doi.org/10.1016/j.molstruc.2019.126995.

Türkkan, B., Özyürek, M., Bener, M., Güçlü, K., Apak, R., 2012. Synthesis, characterization and antioxidant capacity of naringenin-oxime. Spectrochim. Acta Part A Mol. Biomol. Spectrosc. 85 (1), 235–240. https://doi.org/10.1016/j.saa.2011.09.066.

Warad, I., Abdoh, M., Al Ali, A., Shivalingegowda, N., Kumara, K., Zarrouk, A., Lokanath, N.K., 2018a. Synthesis, spectra and X-ray crystallography of dipyridin-2-ylmethanone oxime and its CuX 2 (oxime) 2 complexes: Thermal, Hirshfeld surface and DFT analysis. J. Mol. Struct. 1154, 619–625. https://doi.org/10.1016/j.molstruc.2017.10.087.

Warad, I., Awwadi, F.F., Abd Al-Ghani, B., Sawafta, A., Shivalingegowda, N., Lokanath, N.K., Mubarak, M.S., Ben Hadda, T., Zarrouk, A., Al-Rimawi, F., Odeh, A.B., Barghouthi, S.A., 2018b. Ultrasound-assisted synthesis of two novel [CuBr (diamine)2·H2O]Br complexes: Solvatochromism, crystal structure, physicochemical, Hirshfeld surface thermal, DNA/binding, antitumor and antibacterial activities. Ultrason. Sonochem. 48, 1–10. https://doi.org/10.1016/j.ultsonch.2018.05.009.

Warad, I., Ghazzali, M., Al-Resayes, S., Al-Farhan, K., Al-Othman, Z., 2010. Crystal structure of N-[(methylsulfonyl)oxy]-/Y-((E)-2-(methyl-sulfonyl) oxy]imino-l,2-diphenylethylidene)amine, C16H16N 2O6S2. Z. Krist. – New Cryst. Struct. 225, 611–612. https://doi.org/10.1524/ncrs.2010.0267.

Westcott, B.L., Crundwell, G., Remesic, M., Knopf, K., Chandler, K., McMaster, J., Davies, E.S., 2016. Crystal structure and magnetic properties of di-copper and di-zinc complexes with di-2-pyridyl ketone oxime. Inorg. Chem. Commun. 74, 79–81. https://doi.org/10.1016/j.inoche.2016.11.003.

Wolff, S.K., Grimwood, D.J., McKinnon, J.J., Turner, M.J., Jayatilaka, D., Spackman, M. A., 2012. Crystal explorer.

Zengin, A., Karaoğlu, K., Emirik, M., Menteşe, E., Serbest, K., 2019. Mononuclear Cu (II) complex of an oxime ligand derived from N-Heterocyclic hydrazide: synthesis, spectroscopy, electrochemistry, DFT calculations and catecholase activity. J. Mol. Struct. 1193, 444–449. https://doi.org/10.1016/j.molstruc.2019.05.072.